Extended L-band monolithically tunable InAs/InP quantum-dash multimode laser with integrated amplifier

Emad Alkhazraji,[a,b] Mohd Sharizal Alias,[c] Khurram Karim Qureshi,[d] and Mohammed Zahed Mustafa Khan[a,*]

[a]King Fahd University of Petroleum and Minerals, Optoelectronics Research Laboratory, Electrical Engineering Department, Saudi Arabia

[b]Jubail Industrial College, Department of Electrical and Electronic Engineering Technology, Jubail, Saudi Arabia

[c]Higher Colleges of Technology, Faculty of Engineering Technology and Science, Dubai, United Arab Emirates

[d]King Fahd University of Petroleum and Minerals, Electrical Engineering Department, Dhahran, Saudi Arabia

Abstract. A two-sectioned InAs/InP quantum dash laser structure is proposed and investigated as a monolithic broadband multimodal tunable laser with an integrated semiconductor optical amplifier. The optical power-injection current and spectral characteristics of the device at different operating conditions demonstrated a total wavelength tunability of ∼15.8 nm in the extended-L-band (∼1615 to ∼1630.8 nm) window with ∼2.0 times −3 dB bandwidth enhancement. Furthermore, due to the unique tunability mechanism of forward biasing the amplifier section, the device exhibits simultaneous wavelength tuning as well as optical amplification features, with an estimated gain of ∼8.5 dB affirmed by an increase in the wall-plug efficiency up to 6.8% from 3.9%, shown by its single-section counterpart. This demonstration paves a potential platform for the deployment of broadband quantum-dash laser-amplifiers as unified light sources in next-generation optical access networks. [DOI: 10.1117/1.OE.59.9.096102]

Keywords: quantum dash; tunable laser; optical amplifier.

Paper 20200605 received May 22, 2020; accepted for publication Aug. 14, 2020; published online Sep. 7, 2020.

1 Introduction

With the advent of next-generation wavelength division multiplexing-passive optical networks (WDM-PONs), robust, flexible, and widely wavelength-tunable integrated transmitter modules are paramount in providing high performance at low capital expenditure (CapEx) and operational expenditure (OpEx), while providing protocol transparency in addition to high data rates with limitless scalability.[1] In next-generation WDM-PONs, tunable semiconductor lasers are believed to play a significant role in wavelength-agile networks and as a means to reduce costs as sparing lasers.[2] Moreover, the integration of lasers with semiconductor components, such as amplifiers, modulators, and detectors, becomes increasingly necessary to reduce chip cost, system complexity, and size.[3,4] In addition to optical access networks, high performance and compact tunable sources are indispensable components in applications such as hyper-space imaging, characterization of nanostructures, and in biomedical sensing.[3]

In general, tunable semiconductor laser diodes exhibit single-mode emission and wavelength tunability across the gain profile of the laser's active region via different techniques such as multisectioned devices,[5–8] and external coupled cavities.[9] On the other hand, multimode laser diodes, which are based on Fabry–Perot (FP) cavities, are capable of providing simultaneous emission incorporating several FP modes. Attaining wavelength tuning of such multimode lasers

*Address all correspondence to Mohammed Zahed Mustafa Khan, E-mail: zahedmk@kfupm.edu.sa

0091-3286/2020/$28.00

is very attractive in WDM-PONs,[9] in which, rather than utilizing different broad sources to cover different wavelength groups of optical network units/users (ONUs) wherein each FP mode is assigned as subcarrier to each ONU, a unified tunable multimode laser could be deployed instead, where the broad multimode emission window may be tuned to cover each group of ONUs.[10] Such a unified architecture would enable mass deployment of the transmitter sources and contribute toward the optimization of CapEx and OpEx. This could open a new paradigm toward realization of next-generation WDM-PONs.

In literature, several reports have demonstrated near single-mode wavelength tunability employing external-cavity diode laser configurations that offer broad tuning ranges owing to the wide tunability of the grating rotation angle.[11] However, monolithic semiconductor tunable sources, in the form of superstructure-grating distributed Bragg reflector (DBR), and distributed feedback (DFB) lasers, are more attractive for being compact and monolithically integrable solutions, while providing a good degree of tenability.[12] However, the fabrication of such structures often increases the laser cost significantly, which defeats the low CapEx and OpEx requirements of next-generation passive optical networks (NG-PONs), and hence, a more concrete and cost-effective solution is desirable for practical deployment in varied applications.

Rather than employing DFB, DBR, or grating wavelength filtering elements, semiconductor monolithic tunable lasers could also be realized as multisectioned devices where one section acts as a gain medium while the other section is reverse-biased to act as a saturable absorber section,[1,6] partially injected sections,[5] etc., wherein the active region gain–loss relation is exploited to attain wavelength tunability. Table 1 summarizes different reports of wavelength tunability of semiconductor laser devices. For instance, a continuous multimode wavelength tunability of 12 nm was demonstrated in the C-band (∼1550 nm) over a two-sectioned InGaAsP/InP FP laser diode.[6] On the other hand, exploiting multisectioned devices in slotted[8] and coupled-cavity[13,14]

Table 1 Summary of various wavelength tunability reports in literature.

Device structure	Emission type	Tuning mechanism	Wavelength window	Tunability range	Integrated amplifier	Material system	Ref.
QWell	MM	MS-IL	C-band	2.8 nm	No	—	1
	SM	MS-PP	L-band	12.8 nm	No	InGaAsP/InP	5
	MM	MS	C-band	12 nm	No	InGaAsP/InP	6
	SM	MS-Slotted	C-band	5 channels	No	—	8
	SM	CC	C-band	9 channels	No	InGaAsP/InP	13
	SM	CC	C-band	26 channels	No	InGaAsP/InP	14
QDot	SM	EC	1100 nm	202 nm	No	InAs/GaAs	9
	MM	MS (RB)	1100 nm	7.7 nm	No	InAs/GaAs	20
	MM	MS (RB)	1100 nm	69 nm	No	InAs/GaAs	11
	MM	MS (RB)	1100 nm	83 nm	No	InAs/GaAs	36
	MM	MS (RB)	O-band	45 nm	No	InAs/GaAs	37
	MM	MS (RB)	C-band	110 nm	No	InAs/InGaAsP	21
QDash	SM	IL	L-band	11 nm	No	InAs/InP	19
	MM	EC	L-band	8 nm	No	InAs/InP	22
	MM	MS (RB)	L-band	9.3 nm	No	InAs/InP	23
	MM	MS (FB)	L-band	15.8 nm	Yes	InAs/InP	This work

Note: MM, multimode; SM, single mode; MS, multisection; PP, partially pumped; CC, coupled cavity; EC, external cavity; RB, reverse bias; FB, forward bias.

configurations, a near-single-mode wavelength tunability of up to ∼40 nm was demonstrated on InGaAsP/InP quantum-well (QWell) lasers.

In the past few years, self-organized quantum dot (QDot) and quantum dash (QDash) structures have received attention and have been demonstrating excellent properties, such as compact size, low power consumption, lower threshold current, and integrability in hybrid optical-silicon systems.[15,16] More importantly, these structures are associated with ultrabroad gain profiles due to their highly inhomogeneous sizes and compositions during the self-assembled growth process, unlike their QWell counterparts, which is highly attractive in practical applications.[17,18] Both near-single-mode and multimode tunable lasers have been demonstrated from these low-dimensional nanostructures, as has been summarized in Table 1. For instance, employing external cavity configurations and assisting injection-locking (IL) techniques, near single-mode InAs/GaAs QDot and InAs/InP QDash tunable lasers with a tunability of 202[9] and 11 nm[19] have been reported around 1100 and 1610 nm, respectively. On the other hand, a multimode lasing emission tunability of ∼7.7 nm was reported in Ref. 20 at 1100 nm over an InAs/GaAs QDot laser while a very wide tunability of 110 nm in the C-band was reported over an InAs/InGaAsP QDot tunable laser in Ref. 21. Moreover, in Ref. 22, an optically pumped InAs/InP QDash-based vertical-external-cavity surface-emitting laser demonstrated a multimode tuning range of 8 nm in the L-band. Very recently, we reported a multimode wavelength tunability in the L-band window over a two-sectioned InAs/InP QDash laser diode by reverse-biasing one section resulting in a blueshift tunability of ∼9.3 nm.[23]

One of the main goals of future NG-PONs (NG-PON2 and NG-PON3) is maximizing the per-user capacity and increasing the number of possible subscribers. One of the most promising approaches to realize this is by unrestricting the utilizable bandwidth to the well-exhausted and saturated C-band exclusively and rather extend it to the neighboring L-band as a natural evolution.[24] To that end, L-band QDash-based laser diodes stand out as prime candidates due to their natural emission in the L-band window.

In this work, we exploit the highly inhomogeneous nature of a chirped barrier thickness multilayered InAs/InP QDash structure to realize a monolithic two-sectioned semiconductor laser diode. Contrary to other multisectioned devices in literature wherein wavelength tuning is accomplished via reverse biasing one section, the tunability of our proposed device is carried out by applying positive electric fields across one of the two sections. This can be uniquely performed here owing to the highly inhomogeneous nature of the device's chirped active region, resulting in redshifting the emission wavelength rather than the typical blueshift effect with reverse-biased sections. As such, the device in this work demonstrated a continuous redshift wavelength tunability of ∼15.8 nm from ∼1615 nm, which is, to the best of our knowledge, the largest wavelength tunability range in the mid-L-band. In addition, employing the positive bias wavelength tuning concept has provided an added benefit of amplifying the tunable emission optical power, with a total amplification gain of ∼8.5 dB being demonstrated at a minimal bias voltage of +1.5 V. In addition, the structure's inhomogeneous nature also resulted in the added benefit of a broadened lasing emission spectrum with an observed ∼two-time −3 dB bandwidth enhancement. Consequently, this qualifies the device under investigation here as a monolithic two-sectioned tunable laser with an integrated semiconductor amplifier.

2 Experimental Setup

The integrated tunable laser-amplifier (ITLA) under investigation in this work is a 930-μm-long as-cleaved (reflectivity of ∼0.33) two-sectioned QDash laser diode (QD-LD) whose active region is a chirped four-layered InAs/InP QDash structure each comprising 5 ML of InAs QDashes embedded within 7.6-nm-thick strained $In_{0.64}Ga_{0.16}Al_{0.2}As$ asymmetric QWell layers. Each of the four layers is followed by $In_{0.50}Ga_{0.32}Al_{0.18}As$ QWell top barrier layers whose thicknesses are varied among the different layers to intentionally increase the active region's inhomogeneity and, hence achieve broader gain profiles. In fact, by employing a 77-K photoluminescence (PL) analysis, this chirped barrier thickness QDash laser structure demonstrated a linewidth (full width at half-maximum) of ∼151 nm compared to ∼104 nm from a fixed barrier structure based on the same material system[23] and undergoing identical growth conditions.

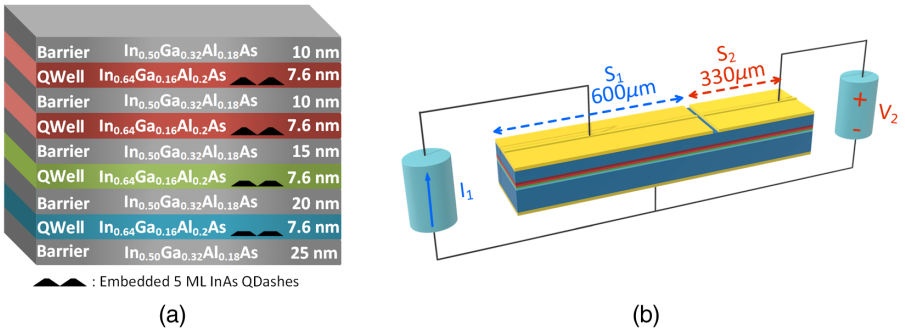

Fig. 1 (a) Epitaxial structure of the chirped active region of the ITLA and (b) an illustration of the ITLA alongside its biasing circuit.

Figure 1(a) shows an epitaxial structure of the chirped active region, whereas more details about the device's structure and fabrication can be found elsewhere.[25] The two segments of the QD-LD are electrically isolated with a measured isolation resistance of $\sim 0.4 - 0.6$ kΩ. The resulting two sections, denoted as S_1 and S_2, are 600- and 330-μm long, respectively, and are separated by a 20-μm-wide trench with a depth matching that of the top p-metal and p-cladding layer (~ 2.3 μm). Figure 1(b) depicts the two-sectioned ITLA alongside its biasing circuitry, where two separate dedicated sources are employed to bias each section independently. Here, S_1 was biased via a pulsed current source (Keithley 2520, I_1) with 0.5 μs pulse-width and a duty cycle of 0.2%, while S_2 is simultaneously forward-biased via a continuous wave (cw) voltage source (Keithley 2400, V_2). In this configuration, S_1 acts as a gain section, whereas S_2 acts as an integrated semiconductor optical amplifier whose gain is controlled by the applied positive voltage V_2. The temperature of the ITLA was controlled via a thermoelectric cooler and was fixed at 15° C to minimize the wavelength drift due to junction heating as much as possible in order to focus on the wavelength tunability of the device due to the dynamics of the active region.

3 Results and Discussion

First, the LI characteristic curves of the ITLA were obtained and plotted in Fig. 2(a) via the S_2 facet output power [the right facet in Fig. 1(b)] under different V_2 settings between 0 and 1.5 V. At first glance, two distinct behaviors can be observed between the different LI curves. For $V_2 \geq 0.6$ V, a typical laser diode LI behavior can be seen, whereas a sharp discontinuity is observed for $V_2 < 0.6$ V at different injection current points. This sharp turn-on behavior is a sign of a highly absorbing system with optical bistability, which has been reported previously on two-sectioned devices.[26,27] Remarkably, this point of transition in the LI behavior ($V_2 = 0.6$ V) signifies the corresponding voltage at which S_2 achieves transparency condition,

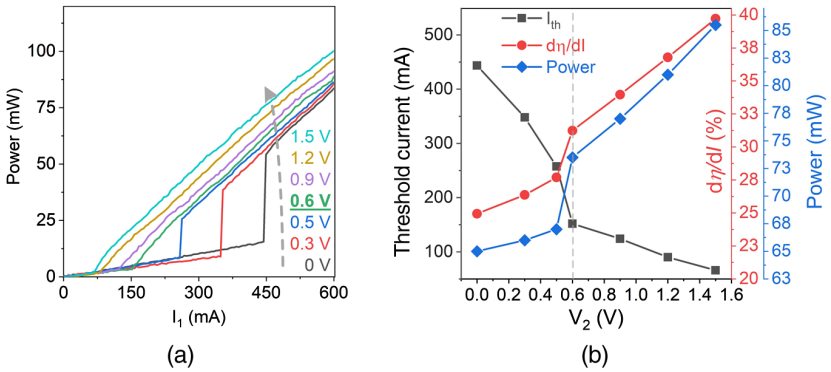

Fig. 2 (a) LI curve of the two-sectioned ITLA under different V_2 settings. (b) The extracted I_{th}, $d\eta/dI$, and optical power as a function of V_2. The dashed line depicts the sharp transition after transparency at $V_2 = \sim 0.6$ V.

that is, no photons absorbed by the material or the loss and the gain in S_2 are balanced. Before this voltage point, S_2 acts as a saturable absorber that absorbs the photons that are emitted from the gain section S_1, that is, most of the emitted photons from S_1, get absorbed in S_2 as long as free carriers are available in S_2. However, at the transparency point and beyond ($V_2 \geq 0.6$ V), the said vacancies are depleted and all the emission from S_1 passes and exits from the facet of S_2 either as is (i.e., at $V_2 = 0.6$ V) or amplified (i.e., for $V_2 > 0.6$ V). In other words, the play-off between the gain-absorption action between S_1 and S_2 is responsible for the bistable behavior observed in Fig. 2(a) for $V_2 < 0.6$ V. Nonetheless, as V_2 is increased to and beyond the transparency point, no more absorptions take place in S_2. It is worth mentioning that the transparency voltage point $V_2 = 0.6$ V is in good agreement with the ~0.59 V value extracted from the fitting of the threshold current density versus inverse cavity length[30], thus affirming the consistency of our analysis.

Furthermore, as V_2 is increased from 0 to 1.5 V, both the optical power (P_o) and differential external quantum efficiency ($d\eta/dI$) increase while I_{th} decreases, as shown in Fig. 2(b). This comes as no surprise since larger positive V_2 values result in a reduced system loss until 0.6 V and after that complement the system gain, and hence the earlier onset of lasing. Moreover, a sharp transition at the transparency point is visible in Fig. 2(b) and is indicated by a dashed line at $V_2 = 0.6$ V. Note that before transparency, both P_o and $d\eta/dI$ increased steadily, followed by a sudden jump in the rate of improvement at the transparency point and later retaining it. On the other hand, an opposite effect is observed in the trend of the threshold current, which is a clear indication of a slowly reducing loss and then an increasing gain from S_2, thus assisting in reaching the overall system gain threshold earlier.

As pointed out earlier, typical two-sectioned semiconductor tunable sources achieve the wavelength tunability by reverse biasing one of the two sections to act as a saturable absorber section whose absorption is altered with reverse biasing, leading to variation in the gain–loss relation of the system, thus blueshifting the emission spectrum. However, due to the quasi zero-dimensional and overlapping density of states (DOS) of the highly inhomogeneous nature of the ITLA's QDash-active region, wavelength redshift tunability is achieved here by virtue of the collective effect of various phenomena such as junction temperature-dependent thermionic emission and carrier leakage, which all have been previously investigated in great detail.[25] To investigate the tunability of the ITLA, the emission spectra were obtained between 1600 and 1640 nm at 15°C under different V_2 values. Figure 3(a) shows the measured spectra at $V_2 = 0$, 0.6 (transparency), and 1.5 V for a fixed current injection condition of 1.1 I_{th} for each case for the sake of comparison under matching operation conditions. The multimodal multipeak nature of the observed at 0 and 1.5 V is a common observation in inhomogeneous QDash[28] structures owing to the complex carrier dynamics of the inhomogeneous QDash-active region that includes photon reabsorption, phonon-assisted tunneling, carrier feeding mechanism, etc. As Fig. 3(a) demonstrates, increasing V_2 results in redshifting the central emission wavelength (calculated as the

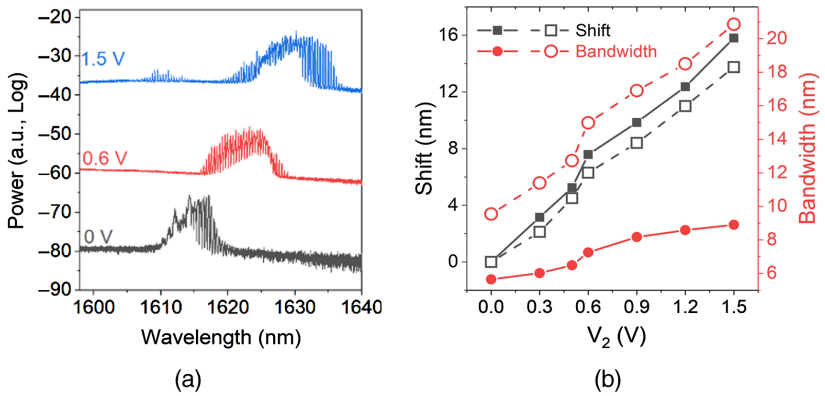

Fig. 3 (a) Emission spectra of the ITLA at a current injection of 1.1 I_{th}, at a temperature of 15°C and under different V_2 values. The spectrums are offset along ordinate for a better view. (b) Summary of the observed redshift and bandwidth of the spectra of the ITLA as functions of V_2 for 1.1 I_{th} (solid lines) and 1.5 I_{th} (dashed lines).

midpoint between the −3 dB points) of the ITLA. Figure 3(b) summarizes these trends as functions of V_2. For instance, as V_2 is increased to 1.5 V, the emission redshifts from ∼1615 to ∼1630.8 nm amounting to a total of ∼15.8 nm, which, to the best of our knowledge, is the highest continuous tunability range reported in the L-band. The redshifting phenomenon is attributed marginally to the device junction heating and chiefly to the reduced loss of the system with increasing V_2. This is ascertained by following the methodology presented in Ref. 25, where the worst-case (assuming entire electrical power dissipated into heat) junction temperature (T_j) rise in S_2 due to the cw injection is calculated to be ∼8.3°C, resulting in an estimated small wavelength redshift of ∼1.6 nm, whereas S_1 exhibits almost no rise in T_j owing to the very small duty cycle (0.2%) pulsed injection.

Furthermore, in the following, we qualitatively shed light on the observed redshift wavelength tunability phenomenon. The threshold gain (g_{th}) of a laser is given as $g_{th} = \alpha_i + \alpha_m$, where α_i is the internal optical losses of the active region due to scattering and absorption, etc., while α_m represents the mirror losses of the cavity, which is fixed for the ITLA. When forward biasing the amplifier section S_2, the onset of lasing can be achieved at a lower current, as observed in Fig. 2. Consequently, if a typical less-inhomogeneous QDash-active-region-based ITLA is considered, the gain peak and, hence the lasing spectrum do not experience much wavelength shift with increasing V_2 values owing to the narrow transition energy band distribution of the QDashes (i.e., dashes with similar heights). Hence, any observation of wavelength redshift in such a case is attributed to heat-induced QDash transition energy shrinkage due to the junction temperature rise. On the other hand, if a highly inhomogeneous QDash-active-region ITLA is considered (i.e., the present work) with widely distributed dash transition energy states, the onset of lasing considerably alters the lasing spectrum. In this case, for smaller V_2 values, the gain peak and hence the lasing wavelength experience a blueshift due to the higher system losses since achieving g_{th} of the system requires carrier recombinations from higher transition energies (i.e., from smaller dashes with larger heights) after filling the lower transition energies (i.e., larger dashes with smaller heights) to compensate for these losses. This results in a lasing emission at a shorter wavelength. However, larger V_2 values reduce the system losses and enable reaching the onset of the lasing from carriers occupying relatively lower transition energy states of larger dashes first, thereby lasing at longer wavelengths. Hence, a redshift in the lasing emission is observed with increasing V_2, which is highly possible in the existing ITLA.

Furthermore, the wavelength tuning of the ITLA was also accompanied by a −3 dB bandwidth broadening from ∼5.6 to ∼8.9 nm at 1.1 I_{th} case, on increasing V_2 from 0 to 1.5 V, as summarized in Fig. 3(b). Remarkably, at a higher injection current of 1.5 I_{th}, this broadening effect is found to be stronger, increasing from ∼9.5 ($V_2 = 0$ V) to ∼21 nm ($V_2 = 1.5$ V), thus translating to a ∼11.5-nm broadening. In general, emission from more fringe larger dashes on the size distribution may achieve population inversion due to the decreasing system losses in addition to a more uniform carrier distribution across the dashes, possibly due to slight thermionic emission, resulting in more wavelength components to emerge and ultimately broadening the emission spectrum.[29] The above phenomenon further intensifies at higher current operation, thereby enabling simultaneous lasing from larger as well as smaller dashes, thus, further broadening the emission bandwidth.[30] With that said, it is worth pointing out that a similar kink in both trends can be observed at the transparency point, indicating the swing in the operation of the device.

Owing to the unique method of achieving wavelength tunability of the device under investigation here (i.e., via forward biasing), S_2 also acts as an integrated semiconductor optical amplifier that provides amplification to the lasing emission generated in S_1. This is evidenced by the higher measured optical powers of the ITLA for larger V_2 values from Fig. 2(a). In literature, such an integration of an optical amplifier in a multisectioned device configuration has been demonstrated over a DBR InAs/InP QDash mode-locked laser in the C-band (∼1545 nm) with an effective gain of ∼10 dB.[31–33] To estimate the amplification action here, the effective gain of S_2 is calculated as the ratio between the optical power (P_o) at any applied driving voltage V_2 and the optical power at transparency (P_t), which is expressed as $g_{eff} = P_o/P_t$. As such, the effective gain of the ITLA was obtained for V_2 values that are above transparency, namely 0.9, 1.2, and 1.5 V, and is plotted in Fig. 3(a) as a function of I_1. It can be seen that g_{eff} of the ITLA saturates around $I_1 = \sim 175$ mA for all V_2 values. Figure 4(b) plots the effective gain at this I_1 value as a function of V_2. A maximum g_{eff} value of 8.5 dB is achieved at $V_2 = 1.5$ V. Moreover,

a closer observation of the trend shows that the effective gain provided by S_2 has not reached saturation, and hence is expected to provide even more effective gain with $V_2 > 1.5$ V. This is due to the features of QDashes that are in between QWells and QDots with relatively larger active region volumes as well as exhibiting quasi zero-dimensional DOSs that enabled the attainment of high effective gain at small applied voltage values.

The amplification taking place in S_2 originates from the increase in g_{eff} via stimulated emission as the optical mode travels through the active region of S_2 and contributes to the optical transition of the electrically injected carriers in the conduction band.[34] Much like semiconductor amplifiers, g_{eff} depends on the injection current. The stimulated photons possess transition energies matching that of the original optical signal, thus amplifying the optical signal with the same wavelength components.[35]

Figure 5(a) depicts the voltage versus current ($I - V$) curves of both sections of the ITLA, namely S_1 and S_2. Due to its smaller size, it can be observed that the measured voltage across S_2 is considerably greater than the measured value across S_1 at any given injection current value. Next, the $I - V$ data were used to obtain the total electrical input power of the ITLA as $P_E = I_1V_1 + I_2V_2$. Then, the wall-plug efficiency (WPE) of the device is obtained as WPE $= P_o/P_E$, where P_o is the output front-facet optical power of the ITLA. As such, Fig. 5(b) shows the obtained WPE of the ITLA for different V_2 values above the transparency point. When comparing Figs. 4(b) and 5(b), it is noteworthy that the ITLA's WPE exhibits a very similar trend to that of the g_{eff} with increasing V_2, which is expected as g_{eff} essentially dictates the amplification, and hence the front-facet output power of ITLA.

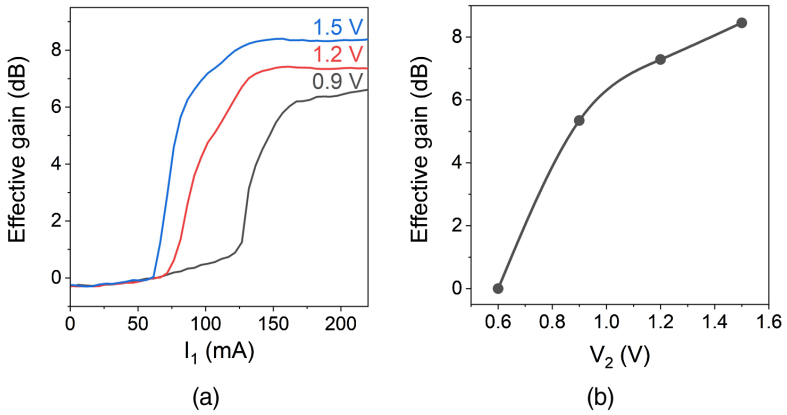

Fig. 4 (a) The effective gain of the ITLA as a function of I_1 for different V_2 settings. (b) The saturated effective gain of the ITLA at $I_1 = 175$ mA as a function of V_2.

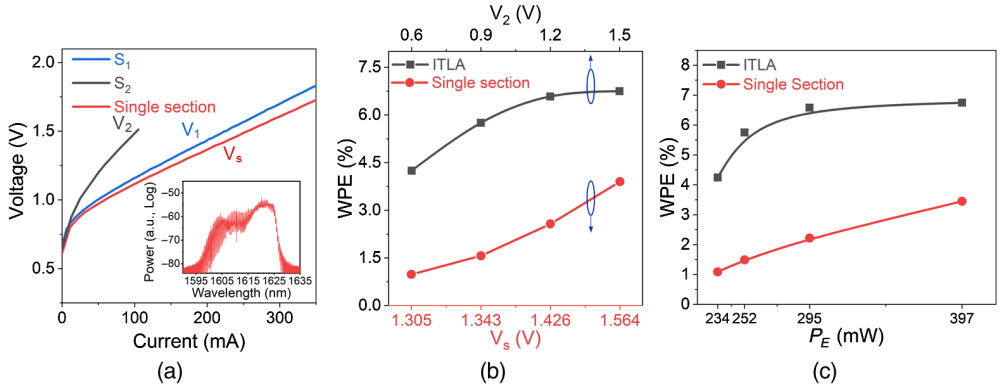

Fig. 5 (a) Voltage versus current ($I - V$) relations of S_1 and S_2 of the ITLA and of the single-section case. The inset of (a) shows the 1.5 I_{th} emission spectrum of the single-section case. (b) The WPE of the ITLA as a function of V_2 and of the single-section case as a function of V_s. (c) The WPE of the ITLA and single-section device under identical input electrical powers.

Next, both sections of the ITLA were electrically shortened together to be uniformly injected by a single current source. In this configuration, the device acts as an ordinary single-section 930-μm-long laser diode in which the whole cavity acts as an active region. Figure 5(a) shows the measured $I-V$ curve of this single-section device. The inset of Fig. 5(a) shows the 1.5 I_{th} emission spectrum ITLA single-section case showing a −3-dB bandwidth of ∼5.8 nm. Thereafter, the WPE of the single-section device is compared with the ITLA to investigate the amplification effect.

This is carried out by operating the single-section device at various current values $I_s = I_1 + I_2$ as a function of I_2 and hence V_2, which would be identical to the total current $(I_1 + I_2)$ operation of the ITLA, and measuring the corresponding single-section voltage (V_s). Finally, the electrical power of the single-section device is found by $P_{E,s} = I_s V_s$. As such, Fig. 5(b) shows the obtained WPE of the single-section case against each V_s value corresponding to each V_2 setting of the ITLA while both the devices operate at identical total injection current. Interestingly, the effect of the amplification action in the ITLA can be witnessed and verified by the higher observed WPE of the ITLA compared to the single-section case. For instance, a WPE of 6.8% was measured from the ITLA ($I_1 = 175$ mA, $V_1 = 1.37$ V, $I_2 = 105$ mA, and $V_2 = 1.5$ V), while the single-section case showed a WPE of 3.9% when operated at the same total current of $I_s = I_1 + I_2 = 280$ mA with a measured V_s of 1.564 V. In other words, with the aid of the integrated semiconductor optical amplifier section, the ITLA is able to generate more photons than the case when it is operated as a single-section device injected with the same electrical current. This is further affirmed by examining the WPE efficiency of both the ITLA and its single-section counterpart under identical electrical input powers, which is depicted in Fig. 5(c). As expected, the ITLA showed significantly higher WPE for any given input power than the single-section device. For instance, a WPE of ∼6.8% was obtained from the ITLA under an input electrical power of 397 mW, while the single-section device showed ∼3.5% under the same electrical input power. This indicates that more photons are able to eject from the ITLA compared to the single-section device under any input power, signifying the effect of the amplification action, owing to the integrated semiconductor amplifier section.

4 Conclusion

We investigated a two-section InAs/InP quantum-dash laser as a tunable laser with an integrated semiconductor optical amplifier. A large redshift wavelength tunability, reaching a value of ∼15.8 nm in the extended-L-band wavelength window with ∼2.0 times improvement in the emission bandwidth broadening, is demonstrated. Moreover, the amplifier section exhibited an effective gain of as high as ∼8.5 dB in addition to controlling the wavelength tunability at 1.5 V forward bias voltage. Furthermore, the amplification action of the ITLA was verified in the form of a significant increase in the WPE (6.8%) when compared to a single-section device of the same length operated at the same injection current (3.9%). Thus, these results reinforce the potential of employing this unique two-sectioned device as an ITLA light source in WDM optical access networks providing wavelength tunability as well as optical power amplification concurrently in the extended L-band region.

Acknowledgments

E.A., K.K.Q., and M.Z.M.K. thank Deanship of Research, King Fahd University of Petroleum and Minerals, for supporting this work through Grant No. IN171029.

References

1. J. Kim et al., "High-capacity DWDM-PON using triple-contact F-P LDs," *IEEE Photonics Technol. Lett.* **23**(2), 127–129 (2011).
2. D. C. Byrne et al., "Discretely tunable semiconductor lasers suitable for photonic integration," *IEEE J. Sel. Top. Quantum Electron.* **15**(3), 482–487 (2009).

3. L. A. Coldren, "Monolithic tunable diode lasers," *IEEE J. Sel. Top. Quantum Electron.* **6**(6), 988–999 (2000).
4. D. F. Welch et al., "The realization of large-scale photonic integrated circuits and the associated impact on fiber-optic communication systems," *J. Lightwave Technol.* **24**(12), 4674–4683 (2006).
5. K. Liu et al., "L-band wavelength-tunable MQW Fabry–Pérot laser using a three-segment structure," *IEEE Photonics Technol. Lett.* **25**(18), 1754–1757 (2013).
6. N. A. Pikhtin et al., "Two-section InGaAsP/InP Fabry–Perot laser with a 12 nm tuning range," *Tech. Phys. Lett.* **23**(3), 214–216 (1997).
7. K. Ah-Hyun et al., "Laser spectral envelope control using a double contact Fabry–Perot laser diode for WDM-PON," *IEEE Photonics Technol. Lett.* **18**(20), 2132–2134 (2006).
8. F. Smyth et al., "Fast wavelength switching lasers using two-section slotted Fabry–Perot structures," *IEEE Photonics Technol. Lett.* **18**(20), 2105–2107 (2006).
9. K. A. Fedorova et al., "Broadly tunable high-power InAs/GaAs quantum-dot external cavity diode lasers," *Opt. Express* **18**(18), 19438–19443 (2010).
10. J. N. Kemal et al., "Coherent WDM transmission using quantum-dash mode-locked laser diodes as multi-wavelength source and local oscillator," *Opt. Express* **27**(22), 31164–31175 (2019).
11. L. Xue-Qin, J. Peng, and W. Zhan-Guo, "A broadband external cavity tunable InAs/GaAs quantum dot laser by utilizing only the ground state emission," *Chin. Phys. B* **19**(1), 018104 (2010).
12. J. E. Johnson et al., "Monolithically integrated semiconductor optical amplifier and electro-absorption modulator with dual-waveguide spot-size converter input," *IEEE J. Sel. Top. Quantum Electron.* **6**(1), 19–25 (2000).
13. Y. Wang, Y. Yang, and J. He, "Single-electrode controlled four-section coupled-cavity tunable laser," *IEEE Photonics Technol. Lett.* **25**(14), 1340–1343 (2013).
14. J. Jin et al., "Widely wavelength switchable V-coupled-cavity semiconductor laser with ~40 dB side-mode suppression ratio," *Opt. Lett.* **36**(21), 4230–4232 (2011).
15. G. Liu et al., "Passively mode-locked quantum dash laser with an aggregate 5.376 Tbit/s PAM-4 transmission capacity," *Opt. Express* **28**(4), 4587–4593 (2020).
16. Z. Lu, *Quantum-Dot Coherent Comb Lasers for Terabit Optical Networking Systems*, SPIE Press, Bellingham, Washington, DC (2019).
17. H. S. Djie et al., "Ultrabroad stimulated emission from quantum-dash laser," *Appl. Phys. Lett.* **91**(11), 111116 (2007).
18. C. L. Tan et al., "Wavelength tuning and emission width widening of ultrabroad quantum dash interband laser," *Appl. Phys. Lett.* **93**(11), 111101 (2008).
19. M. A. Shemis et al., "Broadly tunable self-injection locked InAs/InP quantum-dash laser based fiber/FSO/hybrid fiber-FSO communication at 1610 nm," *IEEE Photonics J.* **10**(2), 1–10 (2018).
20. M. Feng et al., "Wavelength bistability in two-section mode-locked quantum-dot diode lasers," *IEEE Photonics Technol. Lett.* **19**(11), 804–806 (2007).
21. C. N. Allen et al., "External-cavity quantum-dot laser tunable through 1.55 μm," *Appl. Phys. Lett.* **88**(11), 113109 (2006).
22. S. Pes et al., "Class-A operation of an optically-pumped 1.6 m-emitting quantum dash-based vertical-external-cavity surface-emitting laser on InP," *Opt. Express* **25**(10), 11760–11766 (2017).
23. E. Alkhazraji et al., "Monolithic tunable InAs/InP broadband quantum-dash laser," *IEEE Access* **8**, 39046–39055 (2020).
24. D. Nesset, "PON roadmap [invited]," *IEEE/OSA J. Opt. Commun. Networking* **9**(1), A71–A76 (2017).
25. E. Alkhazraji et al., "Effect of temperature and ridge-width on the lasing characteristics of InAs/InP quantum-dash lasers: a thermal analysis view," *Opt. Laser Technol.* **98**, 67–74 (2018).
26. M. J. R. Heck et al., "Observation of Q-switching and mode-locking in two-section InAs/InP (100) quantum dot lasers around 1.55 μm," *Opt. Express* **15**(25), 16292–16301 (2007).

27. G. Farrell, P. Phelan, and J. Hegarty, "Selfpulsation operating regime for absorber of twin section laser diode," *Electron. Lett.* **27**(16), 1403–1405 (1991).
28. C. Ngo et al., "Investigation of semiconductor quantum dots for waveguide electroabsorption modulator," *Nanoscale Res. Lett.* **3**(12), 486 (2008).
29. E. Alkhazraji, M. S. Alias, and M. Z. M. Khan, "Multi-stack chirped InAs/InP quantum-dash structure as a tunable laser," in *Asia Commun. and Photonics Conf.*, pp. 1–3 (2018).
30. E. Alkhazraji et al., "Integrated InAs/InP quantum-dash laser-amplifier," in *Asia Commun. and Photonics Conf.*, Optical Society of America, Chengu, China (2019).
31. S. Joshi et al., "Quantum dash based single section mode locked lasers for photonic integrated circuits," *Opt. Express* **22**(9), 11254–11266 (2014).
32. S. Joshi et al., "Mode locked InAs/InP quantum dash based DBR Laser monolithically integrated with a semiconductor optical amplifier," in *Int. Conf. Indium Phosphide and Related Mater.*, pp. 1–2 (2013).
33. S. Joshi et al., *Mode-Locked InAs/InP Quantum-Dash-Based DBR Laser with Monolithically Integrated SOA*, SPIE Press, Bellingham, Washington, DC (2014).
34. M. J. Connelly, *Semiconductor Optical Amplifiers*, Springer Science & Business Media, Berlin, Germany (2007).
35. C. Shen et al., "Semipolar InGaN quantum-well laser diode with integrated amplifier for visible light communications," *Opt. Express* **26**(6), A219–A226 (2018).
36. A. Biebersdorf et al., "Tunable single and dual mode operation of an external cavity quantum-dot injection laser," *J. Phys. D Appl. Phys.* **36**(16), 1928–1930 (2003).
37. D. I. Nikitichev et al., "High-power wavelength bistability and tunability in passively mode-locked quantum-dot laser," *IEEE J. Sel. Top. Quantum Electron.* **19**(4), 1100907 (2013).

Emad Alkhazraji received his BS and MS degrees and PhD in electrical engineering from King Fahd University of Petroleum and Minerals (KFUPM), Saudi Arabia, in 2014, 2016, and 2020, respectively. Since 2016, he has been a lecturer with the Department of Electrical and Electronic Engineering Technology, Jubail Industrial College, Saudi Arabia. From 2014 to 2016, he was a research assistant with the Electrical Engineering Department at KFUPM. His research focus is on semiconductor QDash lasers and their applications in optical communications.

Mohd Sharizal Alias received his PhD (microengineering and nanoelectronics) from the National University of Malaysia in 2010, and his MSc (physics) and BSc (physics) degrees from the University of Malaya in 2005 and 2000, respectively. He is a faculty member of the Electrical Engineering Department at Higher Colleges of Technology, Dubai, UAE. Prior to that, he was a postdoctoral researcher at Department of Materials, University of Oxford, UK (2018 to 2019). From 2013 to 2018, he was a research scientist at King Abdullah University of Science and Technology, Saudi Arabia. Before joining academia, he was a principal researcher at Telekom Malaysia Research and Development from 2003 to 2013. His research focuses on the usage of nanophotonics to enhance light manipulation for photonic devices. His other research interests include semiconductor lasers and micro-/nano-fabrication process.

Khurram Karim Qureshi received his BSc degree with honors in electrical engineering from the University of Engineering and Technology, Pakistan, in 1999, and his PhD in electrical engineering from the Hong Kong Polytechnic University in 2006. Currently, he is an associate professor in the Electrical Engineering Department of KFUPM. His research interests include tunable semiconductor and fiber-based lasers and fiber sensors.

Mohammed Zahed Mustafa Khan received his BE degree from Osmania University, India, in 2001, MS degree and PhD in electrical engineering from KFUPM and King Abdullah University of Science and Technology (KAUST), Saudi Arabia, in 2004 and 2013, respectively. From 2014 to 2015, he was a SABIC postdoctoral research fellow with Photonics Laboratory, KAUST. Since 2015, he has been an associate professor of electrical engineering, KFUPM. His prior research involved developing numerical models for integrated optical device simulation. Currently, his research focus is on the development of near-infrared and visible semiconductor lasers and systems for applications in optical communications. Khan is a member of the Optical Society of America.